Aeroelastic Analysis of a Helicopter in Steady Maneuver using Dynamic Wake/Dynamic Stall Models

Session subject – Dynamics

M Rohin Kumar, Graduate student, rohin@iitk.ac.in
and
C. Venkatesan, Professor and Head, cven@iitk.ac.in
Department of Aerospace Engineering,
Indian Institute of Technology, Kanpur, India, 208016

Abstract

This paper describes the development of a comprehensive analysis for helicopter aeroelastic analysis including the rotor-fuselage coupling, presents some validation studies and examines the flight dynamics of the helicopter in a steady, level, turning maneuver. The helicopter modeled is a conventional one with a hingeless single main rotor and single tail rotor. The blade undergoes flap, lag, torsion and axial deformations and is modeled using beam finite elements. Tip sweep, pretwist, precone, predroop, torque offset and root offset are included in the model. Aerodynamic model includes Peters-He dynamic wake theory for inflow and the *modified* ONERA dynamic stall theory for airloads calculations. The complete 6-dof nonlinear equilibrium equations are solved for analyzing general flight conditions including steady, level turn. For steady level turns, it is shown that mathematically, three independent approaches exist for the solution of trim equations. The three approaches correspond to setting any one of the three parameters, namely, the lateral acceleration, the sideslip or the track angle equal to zero. Results from the three different solution procedures are presented. It is shown that these three approaches provide different trim quantities leading to several interesting observations.

1. INTRODUCTION

Helicopter simulation is a complex field involving rotary-wing aeroelasticity as well as flight dynamics. Rotary-wing aeroelasticity involves the study of interaction between the structural, inertia and aerodynamic operators. The structural dynamic modeling of the coupled bending, torsion, and axial deformation of helicopter rotor blades has already reached a high level of maturity making use of finite element or multibody techniques. With new generation rotor blades incorporating tip sweep and anhedral angles for performance improvement, later structural dynamics models have accounted for these advanced geometry effects[1,2]. The aerodynamic operator formulation involves the determination of the inflow at the rotor disk and then the calculation of the airloads on the rotor blades. Methods for calculating the inflow range in complexity from the uniform inflow model to dynamic inflow/wake[3] and free-wake models. The most complicated aspect of the unsteady aerodynamics environment is the dynamic stall phenomenon. For accurate airloads calculation, dynamic stall modeling has to be included in the formulation. It is difficult to predict stall and its effects using theoretical unsteady aerodynamic tools. Hence, many researchers still depend on empirical or semi-empirical models. The ONERA[4] model is one such semi-empirical dynamic stall model.

The high-fidelity Computational Fluid Dynamics (CFD) / Computational Structural Dynamics (CSD) coupled analyses have improved aeroelastic prediction capability in recent years. In these analyses, loads based on CFD, which can be both unsteady and nonlinear, are used to obtain solutions. The CFD and the CSD codes are coupled by interactively exchanging airloads and blade deformations with each other. A comprehensive review of the state of art in rotorcraft CFD/CSD coupling for trimmed aeroelastic loads solution in forward flight is given by Datta et al[5]. While development of this field can have major benefits in the prediction of rotor loading in the long run, the need for simpler, less time-consuming models for real-time simulations persists.

While hover and steady 1-g level, forward flight conditions have been studied extensively, maneuvering flight studies have been few and far between. However, high-g maneuvers are important to the rotorcraft from both loads and flying qualities point of view. Maneuvers are more complicated than level flight because of additional factors like pitch and roll angular velocities, asymmetrical conditions like sideslip and yaw, which provide the highest lateral load factors. The accurate prediction of loads in maneuvers (even steady ones) is critical for the design of rotorcraft[6,7]. Inability to do so can result in

longer design cycles and cost escalations resulting from frequent design modifications. The rotor and control system are sized by the high loads encountered in high-g turns. Fatigue life of components is estimated using the vibratory loads as the design loads. Limit load factors for the tail boom and directional control systems are also established by these conditions. The steady turning flight is the most basic of maneuvers. The flight dynamics of rotorcraft in steady turning flight was studied by Chen et al[8,9] and Celi et al[10,11]. Recently, the loads encountered by the UH-60A in the unsteady UTTAS pull-up maneuver were studied extensively with fluid-structure interaction analytical models of varying fidelity[12,13,14]. From literature on maneuvers, it has been observed that a steady turn can be described in three different ways. These three descriptions can lead to three different mathematical conditions, namely (i) lateral load factor, n_y (Y/mg) = 0, (ii) sideslip velocity, $\beta_s = 0$ and (iii) track angle, $\chi_e = 0$.

The complexity of helicopter simulation requires the development of a comprehensive analysis program[15,16] that integrates all the disciplines involved in the study and calculates performance, loads, vibrations and handling qualities of the aircraft. Laxman et al.[17] formulated a computational aeroelastic model by integrating the structural model, the dynamic wake model, and the dynamic stall model for the prediction of trim and response of a helicopter rotor system in steady, level, forward flight. The model developed was applicable for a 6-dof helicopter with a conventional configuration of single hingeless main rotor and a single tail rotor. The present study is an extension of this formulation to include rotor-fuselage coupling for maneuver.

The objectives of this paper are (i) present the development of a comprehensive analysis for helicopter including the rotor-fuselage coupling, (ii) validate the formulation, and (iii) analyze the steady turning maneuver and correlate the analytical results with flight test data. The analytical results of maneuver obtained using three different mathematical conditions are also compared with each other. The sections to follow detail the different components of the model, the solution procedure and comparison of analytical results with flight data for validation.

2. BLADE STRUCTURAL MODEL

An elastic rotating beam with constant angular velocity Ω was considered. Blade sweep, precone, predroop, pretwist, root offset and torque offset are included in the model. The beam consists of a straight portion and a tip with sweep and anhedral angles relative to the straight portion. By convention, backward sweep and anhedral angles have been taken as positive. The cross-section of the blade has a general shape with distinct shear center and center of mass. Several coordinate systems and their transformation matrices were defined to fully describe the geometry and deformation of the rotating blade. The non-linear kinematics of deformation was based on the mechanics of curved rods (small strains and finite rotations) with appropriate provision for cross-sectional shear and out-of-plane warping[18].

2.1. Equations of Motion

The nonlinear equations of motion and the corresponding finite element matrices are derived for each beam element using Hamilton's principle:

$$\int_{t_1}^{t_2} (\partial U - \partial T - \partial W_e)\, dt = 0 \tag{1}$$

where ∂ represents a variation.

Assuming the blade to be made of isotropic material, the variation of the strain energy for each beam element is calculated as

$$\partial U = \int_0^{l_e} \iiint_A \begin{Bmatrix} \delta\varepsilon_{xx} \\ \delta\gamma_{x\eta} \\ \delta\gamma_{x\zeta} \end{Bmatrix}^T \begin{bmatrix} E & 0 & 0 \\ 0 & G & 0 \\ 0 & 0 & G \end{bmatrix} \begin{Bmatrix} \varepsilon_{xx} \\ \gamma_{x\eta} \\ \gamma_{x\zeta} \end{Bmatrix} d\eta\, d\zeta\, dx \tag{2}$$

The variation of kinetic energy for each beam element is calculated as

$$\delta T = \iiint_A \rho \vec{V} \,.\, \delta\vec{V}\, d\eta\, d\zeta\, dx \tag{3}$$

2.2. Finite Element Discretization

The blade was modeled by a series of straight beam finite elements along the elastic axis of the blade. Two finite elements at the tip were used to model the sweep and anhedral. Each finite element in the tip can be given a sweep angle and/or anhedral angle independent of the other. Each beam element consists of two end nodes and one internal node at its mid-point, resulting in 14 degrees of freedom representing 4 lag, 4 flap, 3 torsional and 3 axial deformations. Cubic Hermite interpolation polynomials are used for the bending displacement, while quadratic Lagrangian interpolation polynomials are used for torsional rotation and axial deformations. Applying Hamilton's principle to each finite element results in a discretised form of the equations of motion. Special care has been taken in the treatment of the axial degree of freedom and in the integration of the swept tip mass and stiffness element matrices into the global matrices[19].

Panda[19] derived general transformation and constraint relations between two blade elements joined at an angle to each other. The importance of including nonlinearities in transformations was pointed out, especially for large sweep angles. In the current model, the constraint relation is that the tip sweep or anhedral angle does not change during deformation.

2.3. MAPLE® Implementation

In this work, the nonlinear structural dynamic formulation is implemented in the symbolic computational tool[20], MAPLE®. Traditional moderate deflection beam theories are based on ordering schemes. Coordinate transformations in the derivation of kinetic and strain energy contributions result in large number of terms. The ordering schemes allowed one to neglect higher order terms in the structural, aerodynamic and inertia operators in order to bring down the number of terms to manageable quantity. However, ordering scheme is not unique or consistent. Hence, it has to be applied with care and flexibility. Usage of a symbolic package like MAPLE® helps retain all the terms and reduce the approximations, thus eliminating the need for ordering schemes.

A MAPLE® symbolic computation software package was developed to handle the extensive algebraic manipulation procedure. Using MAPLE®, trigonometric identities and term cancellations can be applied to manipulate the algebra to seek as many simplifications as possible. A symbolic computational tool eliminates the need to simplify problems by hand. Using the programming capabilities in this software, a finite element code was developed for the free vibration analysis. The user interface and the graphical capabilities available are sufficiently mature. Thus modeling, simulation and post-processing of data were all conveniently handled using the same software. MAPLE® also has the tools to convert model equations to important target languages like C, C++ or FORTRAN which can be useful for aeroelastic studies.

3. AERODYNAMIC MODEL

The aerodynamic model involves the evaluation of inflow at the rotor disc and the evaluation of sectional aerodynamic loads on the rotor blade. While the comprehensive analysis program has been implemented as modular with multiple options for inflow and loads calculations, for the purpose of this paper, only the Peters-He dynamic wake model[3] for inflow and the ONERA dynamic stall model[4] for loads are discussed. Both these models, by virtue of their being formulated as a set of differential equations are very suitable for aeroelastic calculations.

The Peters-He dynamic wake model is a compact, closed-form formulation with multiple states that allow variation of the inflow in the radial as well as azimuthal directions. While the model allows for multiple states, for the analysis in this paper, three states were used.

The ONERA model describes the unsteady airfoil behaviour in both attached flow and separated flow using a set of nonlinear differential equations. In the unstalled region, it is identical to Theodorsen's unsteady aerodynamic theory except that the lift deficiency function C(*k)* is approximated by a first order rational approximation. The study by Laxman et al[21] concluded that replacing the first order rational approximation by a second order approximation results in a more accurate *modified* ONERA dynamic stall model, and so the second order approximation shall be used in the present analysis.

4. FLIGHT DYNAMICS

The most general steady maneuver in spin mode is depicted in Fig. 1. The spin axis is always directed vertically. In a steady turn, one has a zero rate of change of the orientation angles Θ (pitch) and Φ (roll). The six non-linear algebraic trim equations are given as:

Force equations

(4) $X = m(w\,q - v\,r) + m\,g \sin\Theta$

(5) $Y = m(u\,r - w\,p) - m\,g \cos\Theta \sin\Phi$

(6) $Z = m(v\,p - u\,q) - m\,g \cos\Theta \cos\Phi$

Moment equations

(7) $L = (I_{zz} - I_{yy})\,q\,r - I_{xz}\,p\,q$ (roll)

(8) $M = (I_{xx} - I_{zz})\,r\,p - I_{xz}\,(r^2 - p^2)$ (pitch)

(9) $N = (I_{yy} - I_{xx})\,p\,q - I_{xz}\,q\,r$ (yaw)

where X, Y, Z and L, M, N are the steady forces and moments acting at the c.g of the helicopter, respectively. These forces and moments include contributions from the main rotor, fuselage, tail rotor and empennage

The body-axis angular rates are related to the Euler angles and the turn rate by the following equations:

(10) $p = -\Omega_{ae} \sin\Theta$

(11) $q = \Omega_{ae} \cos\Theta \sin\Phi$

(12) $r = \Omega_{ae} \cos\Theta \cos\Phi$

There are 13 unknowns in the above set of 9 equations, namely the translational velocities (u, v, w), the angular velocities (p, q, r), the pilot input angles (θ_0, θ_{1c}, θ_{1s}, θ_{tr}), the vehicle orientation angles (Θ, Φ) and the turn rate (Ω_{ae}). To solve the above set of equations, the following four variables may be prescribed in advance – flight speed V_f , path angle γ_f , turn rate Ω_{ae} , and sideslip angle β_s. (Fig. 1)

The components of velocity of the helicopter along the body-axes are given by the following relations:

(13) $u = V_f\,(\cos\Theta \cos\gamma_f \cos\chi_e - \sin\Theta \sin\gamma_f)$

(14) $v = V_f\,(\cos\Phi \cos\gamma_f \sin\chi_e + \sin\Phi\,(\sin\Theta \cos\gamma_f \cos\chi_e + \cos\Theta \sin\gamma_f)$

(15) $w = V_f(-\sin\Phi\cos\gamma_f \sin\chi_e + \cos\Phi(\sin\Theta\cos\gamma_f \cos\chi_e + \cos\Theta\sin\gamma_f)$

where the track angle, $\chi_e = \chi - \Omega_{ae}t$ with t being time (Fig. 2)

From eq. (14), the relationship between the track angle[22] (χ_e) and the sideslip angle β_s can be written as:

(16) $\sin\beta_s = \sin\Phi\sin\Theta\cos\gamma_f \cos\chi_e + \sin\Phi\cos\Theta\sin\gamma_f + \cos\Phi\cos\gamma_f \sin\chi_e$

Fixed-wing aircraft, flying in a coordinated turn, have no sideslip (β_s=0) or lateral acceleration (Y/mg=0). But these conditions cannot be met in a helicopter simultaneously. A helicopter flying in a steady turn with zero lateral acceleration will have an inherent sideslip[8,9] and vice versa.

For the solution of the above trim equations, mathematically, three independent approaches exist. These three approaches correspond to setting any one of the three parameters, namely, the lateral acceleration, the sideslip or the track angle equal to zero. The approach to a solution of the trim equations for these three conditions shall be described next.

4.1. Zero Lateral Acceleration

With side force, Y=0 and substituting eqs. (10), (12), (13) and (15) in eq. (5), we get the track angle as the solution of the following quadratic equation after some mathematical simplification:

(17) $\sin\chi_e = -k\chi_4 \pm \sqrt{(k\chi_4^2 - k\chi_5)}$

where

(18) $k\chi_4 = (k\chi_2\, k\chi_3)/(k\chi_1^2 + k\chi_2^2)$

(19) $k\chi_5 = (k\chi_3^2 - k\chi_1^2)/(k\chi_1^2 + k\chi_2^2)$

and the various coefficients are given as:

(20) $k\chi_1 = \cos\Phi\cos\gamma_f$

(21) $k\chi_2 = \sin\Phi\sin\Theta\cos\gamma_f$

(22) $k\chi_3 = (g/\Omega_{ae}V_f)\sin\Phi\cos\Theta$

In this case, since we now have an additional equation (Y=0), we need to prescribe only 3 variables in advance - V_f, γ_f and Ω_{ae}. Given these variables, first, the track angle is solved for and then the trim equations are solved. Only one of the solutions of eq. (17) will be physically valid. That solution which aids in the convergence of the trim equations is the one to be selected. For steady level turns with lateral acceleration zero, only the positive sign in eq. (17) gave a converged solution in both right and left turns. Another point to note here is that the zero lateral acceleration case is not applicable in the limiting case of load factor equal to 1 (turn rate, Ω_{ae} = 0), which is the level forward flight condition. This is because of the helicopter experiencing a side force due to the tail rotor.

4.2. Zero Sideslip Angle

For this case, eq. (16) is used to obtain the following quadratic equation, which can then be solved for the track angle (V_f, γ_f and Ω_{ae} are prescribed in advance).

(23) $\sin\chi_e = -k\chi_9 \pm \sqrt{(k\chi_9^2 - k\chi_{10})}$

where

(24) $k\chi_9 = (-k\chi_7\, k\chi_8)/(k\chi_6^2 + k\chi_7^2)$

(25) $k\chi_{10} = (k\chi_8^2 - k\chi_6^2)/(k\chi_6^2 + k\chi_7^2)$

and the various coefficients are:

(26) $k\chi_6 = \sin\Phi\sin\Theta\cos\gamma_f$

(27) $k\chi_7 = \cos\Phi\cos\gamma_f$

(28) $k\chi_8 = \sin\beta_s - \sin\Phi\cos\Theta\sin\gamma_f$

Of the two solutions of the quadratic eq. (23), the one which satisfies the sideslip angle zero condition is taken as the correct one. For steady level turns, with sideslip angle zero, the negative sign in eq. (23) was found to be applicable for right turns while the positive sign was found to be applicable for left turns. Once the track angle is obtained, the trim equations can be solved for the pilot input and the vehicle attitude angles.

4.3. Zero Track Angle

In this case, the track angle is set to zero. With V_f, γ_f and Ω_{ae} prescribed in advance, the trim equations can be solved. The sideslip angle is then obtained from eq. (16).

5. SOLUTION PROCEDURE

Figure 3 shows the flow chart of the procedure used for the coupled rotor/fuselage trim analysis of a helicopter in general maneuvering flight. For structural dynamics, the rotor blade was modeled using finite elements, with each element having 14 degrees of freedom. Modal coordinate transformation was used to reduce the total number of degrees of freedom. Eight modes comprising of the two lag, four flap, one torsion and one axial modes were used in the modal transformation. The aerodynamic loads were calculated at 15 equidistant stations on the rotor blades. The trim equations comprise the complete nonlinear vehicle force and moment equilibrium equations. The algorithm shown was implemented as a C++ program

using the open-source *GSL*[23] as the math library. The differential equations are solved using the Runge-Kutta method while the non-linear algebraic trim equations are solved using the Newton-Raphson method. The program outputs inflow over the rotor, hub loads, blade response, blade sectional loads, blade shear and bending moments, pilot inputs and the vehicle attitudes.

6. RESULTS

The structural dynamics formulation was validated with the University of Maryland vacuum chamber experiments[24,25,26]. For the validation of the aeroelastic formulation, analytical results for steady, level, forward flight as well as maneuver are compared with flight test data. The vehicle and blade properties are given in Table 1. The rotor of the helicopter turns anticlockwise when viewed from the top.

6.1. Trim for steady level forward flight

Figure 4 shows the variation of trim angles with speed in level forward flight. The analytical results have been correlated with flight data[27]. The main rotor collective, tail rotor collective and the main rotor lateral cyclic angles are in good agreement with the flight test data. However, the main rotor longitudinal cyclic and the vehicle pitch and roll attitudes have been overpredicted. All the predicted trim variables deviate from the flight test data at higher speeds. A possible reason for these discrepancies could be that the rotor inflow aerodynamic interactions with the fuselage and the empennage have not been modeled.

6.2. Trim for steady level turn

In the steady level turn condition, the helicopter velocity is constant and flight path angle γ_f is equal to zero. Figure 5 shows the variations of trim angles with increasing load factors for both left turn and right turn for a speed of 50m/s. Calculations were done assuming the zero sideslip angle case. Sample flight test data for a couple of parameters are also plotted for correlation.

The main rotor collective pitch is seen to be increasing with increase in the load factor. While the tail rotor collective is seen to be increasing with increasing load factor, the rate of increase is higher for the right turn than the left turn. The cyclic angles for the turns do not vary much with change in load factor. The pitch attitude remains more or less the same for different load factors. The roll angle plot shows that the helicopter banks towards the direction of the turn and it increases with increasing load factor, as expected. Overall, it is seen that the main rotor collective and the roll angle prediction correlate well with the flight data.

Figure 6 shows the variation of trim angles with turn rate for all the three cases considered above, namely, zero lateral acceleration, zero sideslip angle and zero track angle for a helicopter velocity of 50m/s. The turn rate has been chosen as abscissa inorder to show both left turn and right turn curves in the same plot. A positive turn rate represents right turn while negative turn rate represents left turn (The relationship between turn rate and load factor is given in Fig. 7). For zero flight path angle, γ_f, the relation between load factor, η_f and turn rate, Ω_{ae} is given as

$$\eta_f = \sqrt{1+\left(\Omega_{ae} * \frac{V_f}{g}\right)^2} \tag{29}$$

A turn rate of 0 deg/s corresponds to load factor of 1 and a turn rate of ±20 deg/s corresponds to a load factor close to 2. In Fig. 6, the breaks in the zero lateral acceleration curves are because of the fact that at zero turn rate, the helicopter cannot have zero lateral acceleration on account of its asymmetry.

The main rotor collective pitch predictions are almost the same for the three cases. It increases with increasing turn rate for both right turn and left turn. The tail rotor collective is predicted almost the same by the zero sideslip and the zero track angle cases. However, for the zero lateral acceleration case, the tail rotor collective predicted is far lesser than in the other two cases. Here, it increases with turn rate during right turns, while in the left turns, it is negative.

The lateral cyclic is also predicted almost the same by the zero sideslip and the zero track angle cases. For the zero lateral acceleration case, the lateral cyclic angle is lesser than those of the other two cases. It increases with increase in turn rate during right turns and decreases with increase in turn rate during left turns. It is also to be noted that for the zero lateral acceleration case, the lateral cyclic angle in a turn is always lesser than that in the level forward flight (i.e. zero turn rate condition)

There is not much difference in the predictions of the longitudinal cyclic in the three cases in the right turn. However, in the left turn the zero lateral acceleration case predicts a higher angles than the other two cases.

The pitch attitude shows a large difference in the predictions by the zero lateral acceleration case as compared to the other two cases, especially during the left turn. While for all the other cases, the pitch attitude is more or less uniform for different turn rates, for the zero lateral acceleration case in the left turn, the pitch attitude becomes increasingly nose-down as the turn rate increases.

The roll attitude shows similar trends and values for all the three cases in the right turn. In the left turn, the zero lateral acceleration case predicts lower angles than the other two cases. For both turns, the roll attitude increases in the same direction as the turn with increase in turn rate.

In Fig. 8a, it is seen that both for the zero track angle case and the zero lateral acceleration case, the helicopter experiences a sideslip angle during a turn. For the zero

track angle case, sideslip angle has only a slight variation with turn rate. It increases with turn rate in right turn and decreases with increase in turn rate during left turn. The result is contrary both in magnitude and trend in the zero lateral acceleration case. Here, sideslip decreases with increase in turn rate in the right turn while it increases in the left turn. The magnitude of trim sideslip angles are also much larger for this case. It is to be noted that at higher positive turn rates (or high load factors in the right turn), both the zero track angle case and the zero lateral acceleration cases give sideslip angles very close to zero. Thus the three cases are seen to be equivalent at high positive turn rates. This is also seen in the results of the trim angles variation in Fig. 6.

The lateral acceleration variation with turn rate (Fig. 8b) shows similar trend for both the zero sideslip angle and the zero track angle cases. It decreases with turn rate in right turn and increases with increase in turn rate during left turn. It is to be noted again that for higher positive turn rates, both the cases have low lateral acceleration close to zero, which again leads to the conclusion that at high positive turn rates, the three trim solution cases are equivalent.

Figure 9 shows the angular velocities of the helicopter in level turn. For the zero track angle and zero sideslip cases, the helicopter rolls away from the turn, i.e, $p<0$ for right turn and $p>0$ for left turn (Fig. 9a). For the zero lateral acceleration case, while for the right turn, $p<0$, for the left turn also $p<0$ with a large magnitude. So the helicopter rolls into the turn in the left turn. Figure 9b shows the pitch angular velocities. For both left and right turns, $q>0$. The three cases give similar results.

7. CONCLUSIONS

A comprehensive analysis capability for a conventional helicopter has been developed and validated for trimmed forward flight. For steady level turns, three different approaches for the trim solutions have been presented. For the zero lateral acceleration case, the lateral cyclic angles in turns are predicted to be always less than that in level forward flight. It has also been shown that at high positive turn rates or , alternatively, at high load factors in the right turn, the three approaches give similar results.

COPYRIGHT STATEMENT

NOMENCLATURE

A	=	Cross-sectional area of the rotor blade, m^2
dt, dx	=	Time step and elemental length
E	=	Young's modulus
G	=	Shear modulus
g	=	acceleration due to gravity (= 9.81 m^2/s)
$I_{xx}, I_{yy},$ I_{zz}, I_{xz}	=	Aircraft mass moments of inertia about body axes at the c.g
L, M, N	=	Components of total moments along body axes at the c.g
m	=	Mass of the helicopter, kg
p, q, r	=	Angular velocities along body axes at the c.g
T	=	Kinetic energy
U	=	Strain energy
V	=	Velocity of the blade point measured in an inertial frame, m/s
V_f	=	Helicopter velocity (Fig. 1)
W_e	=	Virtual work done by non-conservative external forces
u, v, w	=	Velocity components along body axes at the c.g
X, Y, Z	=	Components of the total forces along body axes at the c.g
β_s	=	Sideslip angle (= $\sin^{-1}(v/V_f)$)
ε_{xx}	=	Axial strain
$\gamma_{x\eta}, \gamma_{x\zeta}$	=	Shear strain
γ_f	=	Flight path angle (Fig. 1)
η, ζ	=	Cross-sectional coordinates
η_f	=	Load factor
Ω	=	Rotational speed of the rotor blade, rpm
Ω_{ae}	=	Turn rate of vehicle, rad/s (Fig. 1)
ρ	=	Density of the blade, kg/m^3
Φ	=	Fuselage roll attitude
Θ	=	Fuselage pitch attitude
χ_e	=	Track angle

REFERENCES

[1] Kim, K.C. and Chopra, I., "Aeroelastic Analysis of Swept, Anhedral, and Tapered Tip Rotor Blades," *Journal of the American Helicopter Society*, Vol. 37, No. 1, 1992.

[2] Yuan, K.A., Friedmann, P.P. and Venkatesan, C., "A New Aeroelastic Model for Composite Rotor Blades with Straight and Swept Tips," *33rd AIAA Structural Dynamics & Materials Conference*, AIAA 92-2259, Dallas, Texas, April 1992.

[3] He, Cheng Jian., "Development and Application of a Generalized Dynamic Wake Theory for Lifting Rotors," *Ph.D Dissertation*, Georgia Institute of Technology, July 1989.

[4] Petot, D., "Differential Equation Modeling of Dynamic Stall", *La Reserche Aerospatiale*, Paper No. 1989-5, 1989.

[5] Datta, A., Nixon, M., and Chopra, I., "Review of Rotor Loads Prediction with the Emergence of Rotorcraft CFD", *Journal of the American Helicopter Society*, Vol. 52, No. 4, October 2007.

[6] Engineering Design Handbook, Helicopter Engineering, Part One, Preliminary Design. *AMCP 706-201, US Army Materiel Command*, August 1974.

[7] Engineering Design Handbook, Helicopter Engineering, Part Two, Detail Design. *AMCP 706-202, US Army Materiel Command*, August 1974.

[8] Chen, R.T.N., "Flight Dynamics of Rotorcraft in Steep High-g Turns," *Journal of Aircraft*, Vol. 21, (1), Jan 1984.

[9] Chen, R.T.N. and Jeske, J.A., "Kinematic Properties of the Helicopter in Coordinated Turns," *NASA Technical Paper 1773*, Apr 1981.

[10] Celi, R., "Hingeless Rotor Dynamics in Coordinated Turns," *Journal of the American Helicopter Society*, Vol. 36, No. 4, October 1991.

[11] Ribera, M. and Celi, R., "Simulation modeling in steady turning flight with refined aerodynamics," *31st European Rotorcraft Forum*, Florence, Italy, September 2005.

[12] Abhishek, Datta, A., Ananthan, S., and Chopra, I., "Prediction and Analysis of Main Rotor Blade Loads in a Prescribed Pull-Up Maneuver," *Journal of Aircraft*, Vol. 47, No. 4, July–August 2010

[13] Sitaraman, J. and Roget, B., "Prediction of Helicopter Maneuver Loads Using a Fluid-Structure Analysis," *Journal of Aircraft*, Vol. 46, No. 5, September-October 2009.

[14] Yeo, H., "Investigation of Rotor Airloads and Structural Loads in Maneuvering Flight," *64th Annual Forum, The American Helicopter Society*, Montreal, Canada, April 29 – May 1, 2008.

[15] Kunz, D.L., "Comprehensive Rotorcraft Analysis : Past, Present and Future," *46th AIAA Structural Dynamics & Materials Conference*, AIAA 2005-2244, Austin, Texas, April 2005.

[16] Johnson, W., "Rotorcraft Aeromechanics Applications of a Comprehensive Analysis," *Heli Japan 98: AHS International Meeting on Advanced Rotorcraft Technology and Disaster Relief,* Japan, April 1998.

[17] Laxman, V. and Venkatesan, C., "Influence of Dynamic Stall and Dynamic Wake Effects on Helicopter Trim and Rotor Loads", *Journal of the American Helicopter Society*, Vol. 54, No. 3, July 2009.

[18] Wempner, G., *Mechanics of Solids with Applications to Thin Bodies*, Sijthoff & Noordhoff, 1981.

[19] Panda, B., "Assembly of Moderate-Rotation Finite Elements Used in Helicopter Rotor Dynamics," *Journal of the American Helicopter Society*, Vol. 32, No.4, 1987.

[20] http://www.maplesoft.com/products/Maple/

[21] Laxman, V. and Venkatesan, C., "Chaotic Response of an Airfoil due to Structural Coupling and Dynamic Stall," *AIAA Journal*, Vol. 45, Jan. 2007.

[22] Padfield, G.D., "Helicopter Flight Dynamics: The Theory and Application of Flying Qualities and Simulation Modeling. *AIAA Education Series*, 1996.

[23] GSL – GNU Scientific Library, URL: http://www.gnu.org/software/gsl/

[24] Rohin Kumar, M., Venkatesan, C., "Structural Dynamic Analysis of Helicopter Rotor Blades with Advanced Geometry Tip Shapes," *XVII NASAS*, IIT Kanpur, India, September 2011.

[25] Rohin Kumar, M., Venkatesan, C., "Rotorcraft Aeroelastic Analysis using Dynamic Wake/Dynamic Stall Models and its Validation," *Proceedings of IFASD 2013*, Bristol, UK, June 2013.

[26] Epps, J.J. and Chandra, R., "The Natural Frequencies of Rotating Composite Beams with Tip Sweep," *Journal of the American Helicopter Society*, Vol. 41, no. 1, 1996.

[27] Singh, G., "Helicopter Flight Dynamics Simulation for Analysis of Trim, Stability and Control," *Masters Dissertation*, Department of Aerospace Engineering, Indian Institute of Technology, May 2012.

Table 1 Vehicle and blade properties

Parameter	Symbol	Value	Units
Air density	ρ	0.954	kg/m^3
Main rotor			
Number of blades		4	
Non-dimensional blade chord	c/R	0.0757	
Solidity ratio	σ	0.09646	
Weight coefficient	C_W	0.00734	
Pre-Twist		-12	degrees
Lift curve slope	$c_{l\alpha}$	5.73	
Profile drag coefficient	c_{d0}	0.01	
Lock number	γ	6.4	
Torque offset		0.0015	
Predroop		2.5	degrees
Modal frequencies of rotor blade			
Lag		0.71, 5.30	
Flap		1.09, 2.88, 5.01, 7.57	
Torsion		4.37	
Axial		33.36	
Vehicle			
Equivalent flat plate area		0.0131	
Parasite drag coefficient		1	

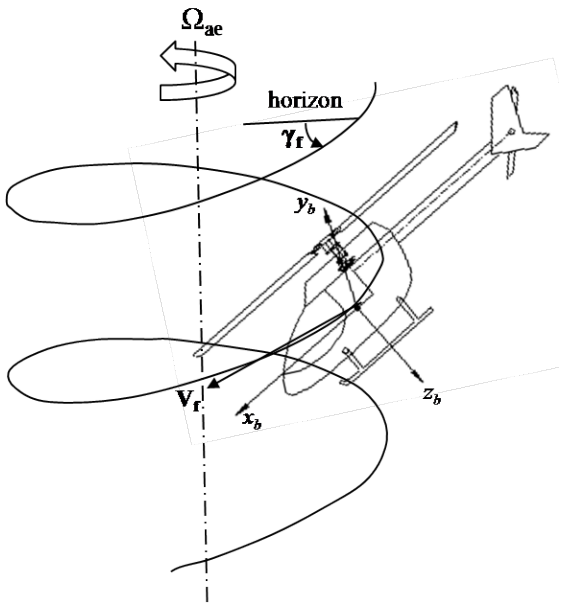

Fig. 1 Helicopter in a general maneuver[22]

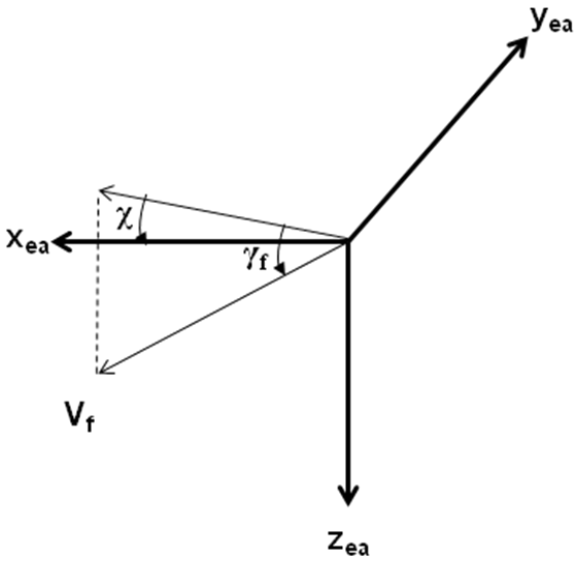

Fig. 2 Velocity vector shown in the fixed Earth axis

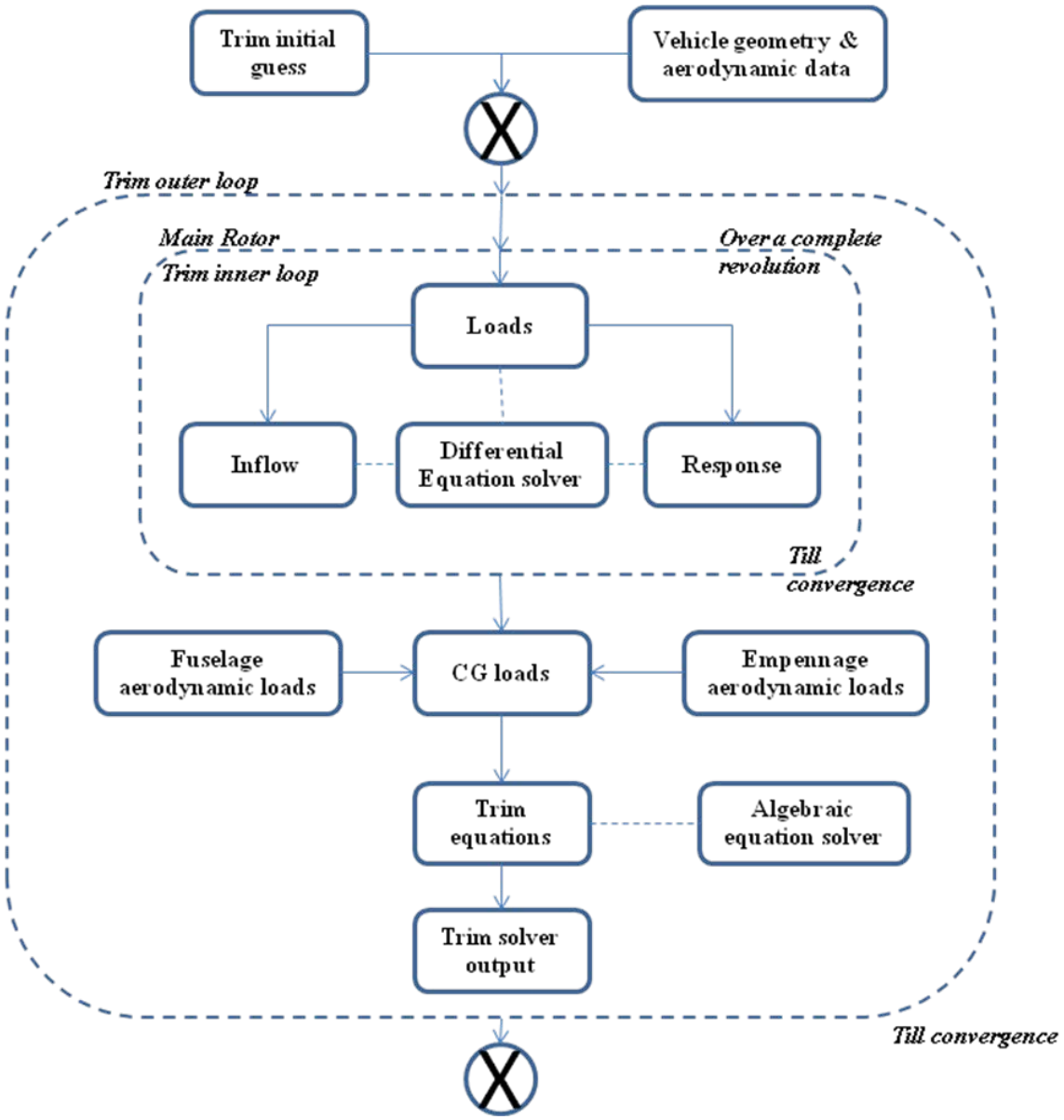

Fig. 3 Flowchart for helicopter trim and rotor response

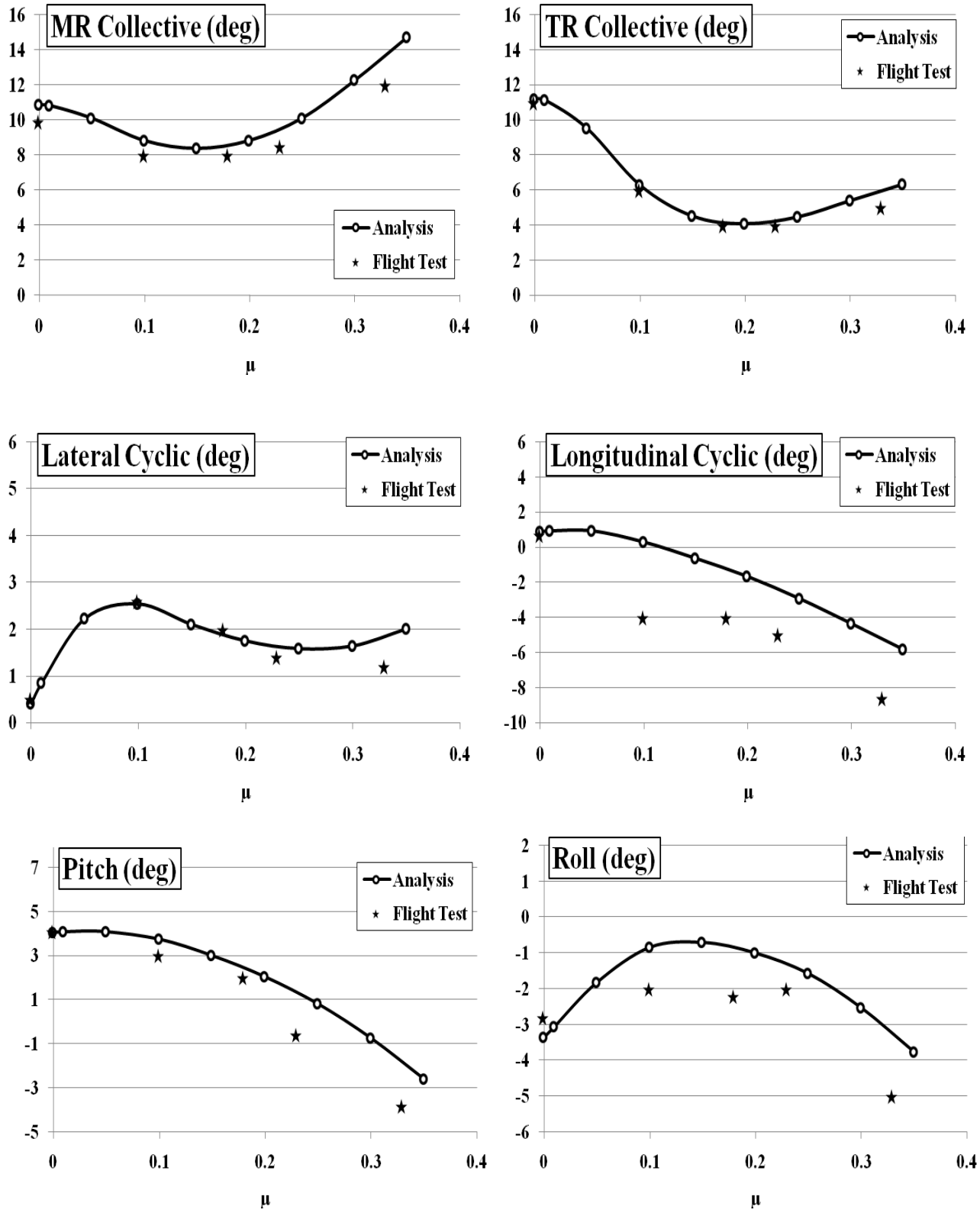

Fig. 4 Comparison of trim angles with flight test data as a function of forward speed in level flight

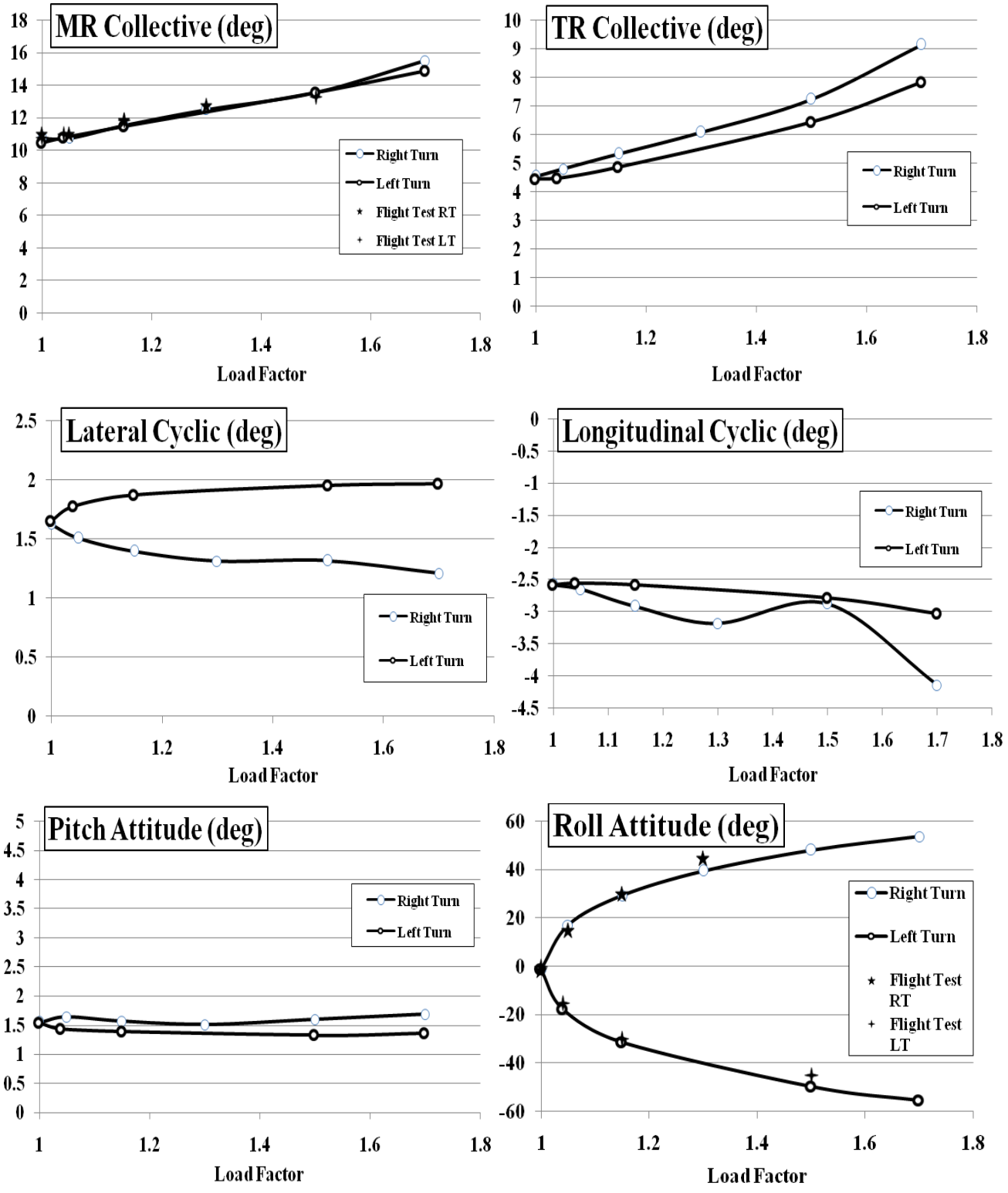

Fig. 5 Trim angles variation with load factor for steady turn @ 50m/s (sideslip β_s=0)
(Comparison with flight test data in main rotor collective and helicopter roll angle)

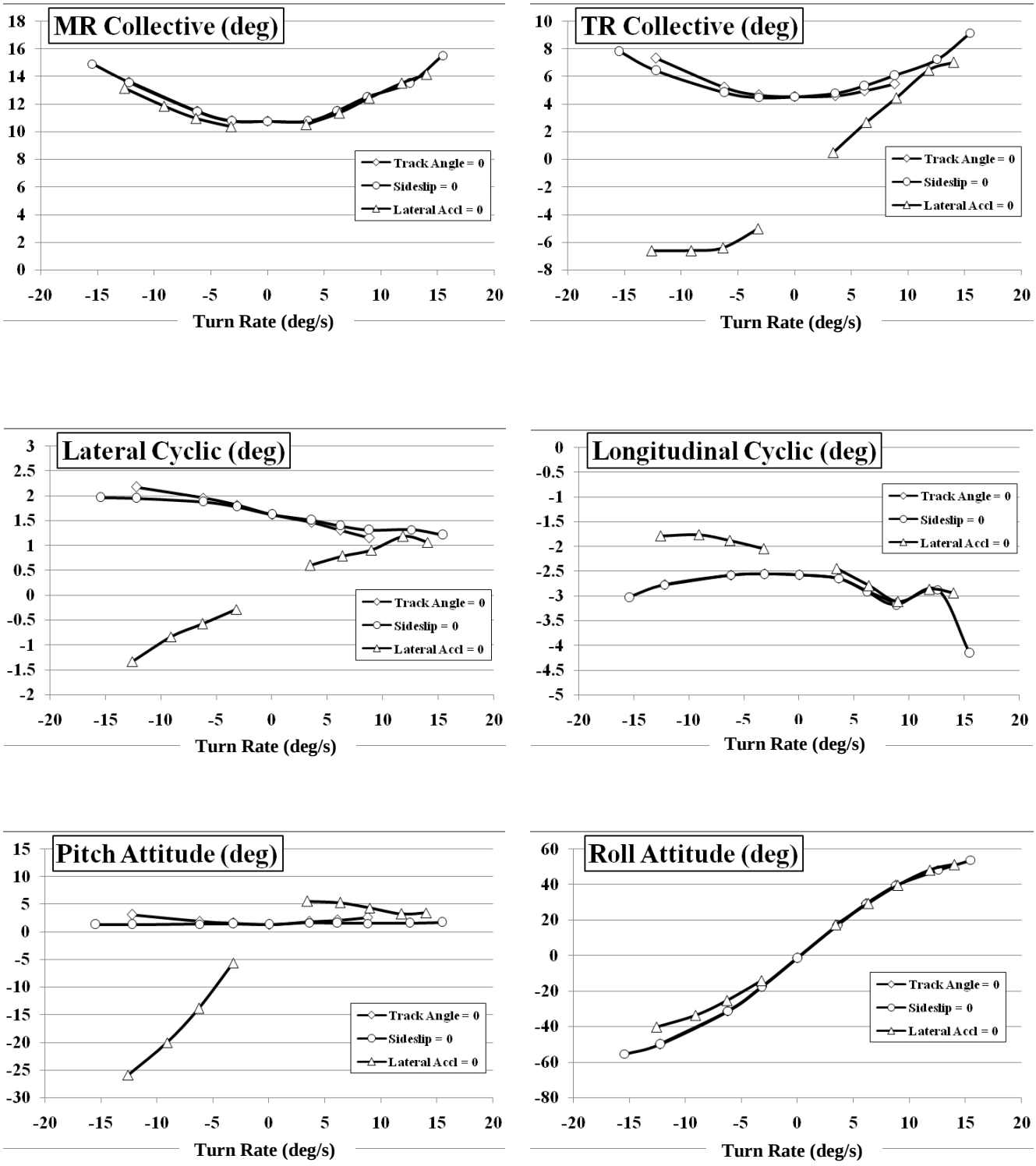

Fig. 6 Trim angles variation with turn rate for steady turn @ 50m/s for three different cases (zero track angle, zero sideslip and zero lateral acceleration)

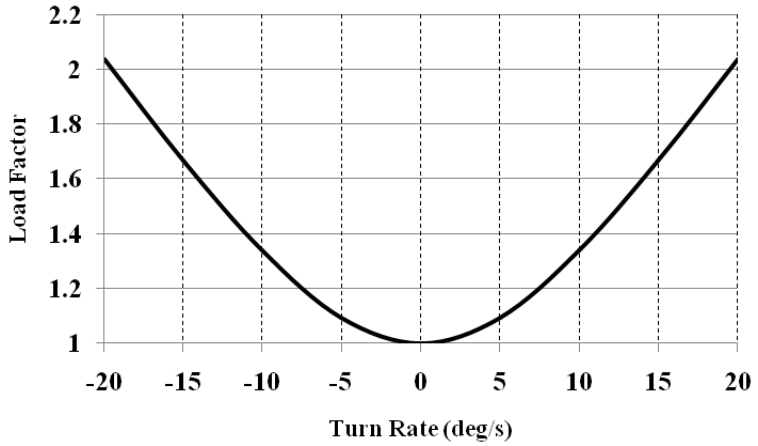

Fig. 7 Relation between load factor and turn rate

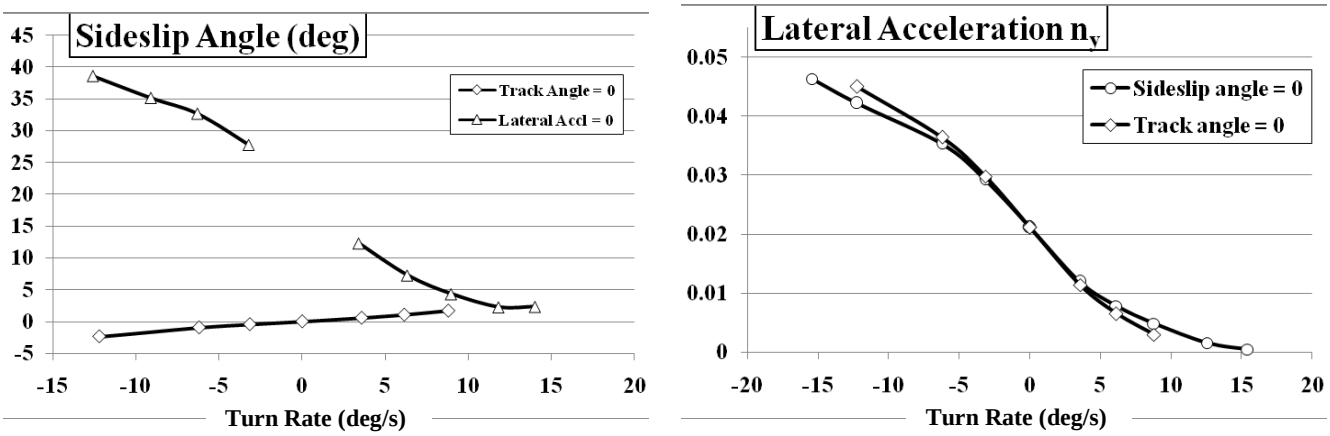

(a) **(b)**

Fig 8. Sideslip angle and lateral acceleration variation with turn rate

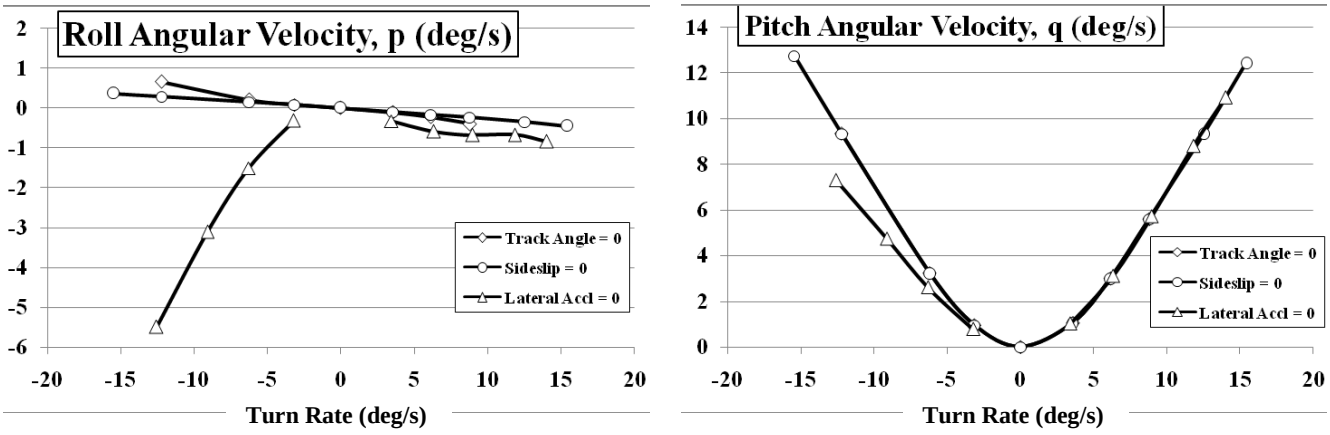

(a) **(b)**

Fig. 9 Roll and Pitch angular velocities variation with turn rate